Distributed MIMO chaotic radar based on wavelength-division multiplexing technology

Tingfeng Yao,[1] Dan Zhu,[1,2] De Ben,[1] and Shilong Pan[1,*]

[1]*The Key Laboratory of Radar Imaging and Microwave Photonics, Ministry of Education, Nanjing University of Aeronautics and Astronautics, Nanjing 210016, China*

[2]*e-mail: danzhu@nuaa.edu.cn*

**Corresponding author: pans@ieee.org*

Received December 8, 2014; revised February 26, 2015; accepted March 9, 2015; posted March 11, 2015 (Doc. ID 229327); published April 3, 2015

A distributed multiple-input multiple-output chaotic radar based on wavelength-division multiplexing technology (WDM) is proposed and demonstrated. The wideband quasi-orthogonal chaotic signals generated by different optoelectronic oscillators (OEOs) are emitted by separated antennas to gain spatial diversity against the fluctuation of a target's radar cross section and enhance the detection capability. The received signals collected by the receive antennas and the reference signals from the OEOs are delivered to the central station for joint processing by exploiting WDM technology. The centralized signal processing avoids precise time synchronization of the distributed system and greatly simplifies the remote units, which improves the localization accuracy of the entire system. A proof-of-concept experiment for two-dimensional localization of a metal target is demonstrated. The maximum position error is less than 6.5 cm.

OCIS codes: (280.5600) Radar; (060.5625) Radio frequency photonics; (350.4010) Microwaves.
http://dx.doi.org/10.1364/OL.40.001631

Multiple-input multiple-output (MIMO) radar which is a radar system employing multiple transmit waveforms and jointly processing signals received at multiple receive antennas has attracted considerable interest in the past decade [1,2]. With widely separated antennas, MIMO radar can overcome the impairments of the target's radar cross section fluctuations by exploiting spatial diversity. Moreover, in conjunction with the centralized processing, MIMO radar has the potential to further enhance the radar performance in detection and parameter estimation. In the distributed MIMO radar, multiple orthogonal waveforms, which are defined as the waveforms with very low cross-correlation and high self-correlation, have to be applied to differentiate the origins of the received signals. Thanks to the sensitivity of the chaotic signal to the initial condition, it is very easy to generate a large number of long-sequence orthogonal waveforms using chaotic systems [3]. In addition, unlike noise, the chaotic signals with good correlation property are deterministic and controllable, which make the chaotic signals well suited for distributed MIMO radar application. However, the chaotic signals generated by electrical circuits are usually bandwidth limited [4]. To overcome this problem, photonic-assisted broadband chaotic signal generation was proposed, which was generally implemented based on the chaotic behavior of photonic nonlinear dynamics in a laser diode (LD) [5–8] or an optoelectronic oscillator (OEO) [9,10].

The other challenge to realize a practical distributed MIMO chaotic radar is the precise time synchronization between the different radar units because all these units are working cooperatively. Furthermore, since the transmitters and the receivers are separated with considerable distances, it is hard to obtain the replicas of the transmitted chaotic signals to realize match filtering in each receiver [11]. Therefore, centralized processing of the raw data from all receivers is highly desirable. However, the receivers are conventionally connected to a central station by electrical cables, which always have limited bandwidth and large transmission loss, and further restrict the bandwidth and coverage of the radar. Recently, several photonic technology based sensor networks to realize high accuracy localization have been reported [12,13]. Thanks to the advantages brought by the photonic techniques, such as low loss, immunity to electromagnetic interference, and broad bandwidth, all the received signals can be sent directly to the central station for joint processing, so the signal processing is moved from each sensor node to the central station, which significantly simplifies the entire system and increases the localization accuracy.

In this Letter, we propose and demonstrate a novel concept to realize a distributed MIMO chaotic radar without complex signal processing and precise clock synchronization in each receiver based on wavelength-division multiplexing (WDM) technology. The wideband quasi-orthogonal chaotic signals are generated by chaotic OEOs. All of the reference signals from the transmitters and the received signals from the receivers are sent to the central station via a WDM network for joint processing. Because of the centralized signal processing and fixed fiber lengths between the radar units and the central station, clock synchronization of the radar units is not required. A proof-of-concept experiment is carried out for two-dimensional localization of a metal target. The position error is within 6.5 cm.

The schematic diagram of the proposed distributed MIMO chaotic radar is shown in Fig. 1, which comprises a central station, several transmitter remote units, and several receiver remote units. Each transmitter unit contains a chaotic OEO and an ultra-wideband (UWB) antenna. The chaotic OEO consists of an LD, a Mach–Zehnder modulator (MZM), a length of single mode fiber (SMF), a photodetector (PD), a UWB electronic bandpass filter (EBPF), and a high-power electrical amplifier (EA). An optical splitter is inserted after the MZM to tap out some of the optically modulated chaotic signal as a reference signal, and an electrical coupler is used to

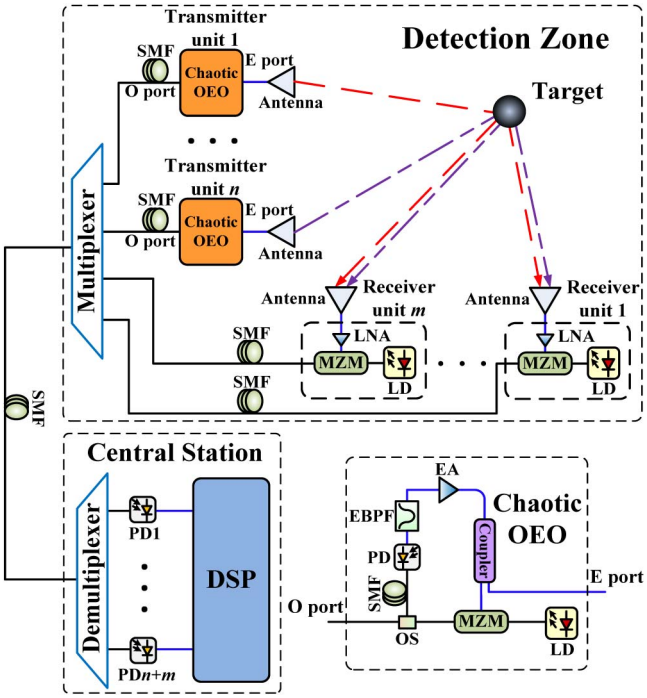

Fig. 1. Schematic diagram of the proposed distributed MIMO chaotic radar based on WDM technology. LD, laser diode; MZM, Mach–Zehnder modulator; OS, optical splitter; SMF, single-mode fiber; PD, photodetector; EBPF, electrical bandpass filter; EA, electrical amplifier; LNA, low noise amplifier.

introduce part of the chaotic signal to the UWB antenna as the emission signal. The dynamics of the chaotic OEO can be described by a delay differential equation: [10]

$$\left(1+\frac{\tau}{\theta}\right)x+\tau\frac{dx}{dt}+\theta^{-1}\int_{t_0}^{t}x(s)\mathrm{d}s=mT(x(t-\tau_D)), \quad (1)$$

where $\tau=1/2\pi f_H$ and $\theta=1/2\pi f_L$ denote the characteristic time scale of the high-frequency cutoff and low-frequency cutoff, respectively; f_H and f_L are determined by the passband of the EBPF; m is the normalized gain in the loop; and τ_D is the time delay of the loop. When the feedback gain is large enough, the OEO will fall into chaotic oscillation, and a chaotic signal could be generated. Since for different chaotic OEOs, the oscillation is from different initial states, the chaotic signals generated by different chaotic OEOs are quasi-orthogonal [3].

Each receiver unit is composed of a UWB antenna to receive the signal scattered from the target, a low noise amplifier (LNA) to amplify the received signal, and an MZM and an LD to convert the received signal to be an optical signal. Then, the received signals are sent to the central station with the reference signals by using WDM technology. It should be noted that the received signal from each receiver unit contains the scattered signals from all the transmitters. Thanks to the quasi-orthogonal property of the chaotic signals, the signal from each transmitter can be differentiated.

The target location is determined by the time of arrivals (TOAs) from multiple transmitters to multiple receivers. For a stationary target, each TOA defines an ellipse in which the target must lie. Thus, the target location is found out by the intersection of a set of TOA defined elliptical curves for two-dimensional localization. A typical two-dimensional localization scenario using two transmitters and two receivers is shown in Fig. 2. From the above analysis, we can obtain the following relations:

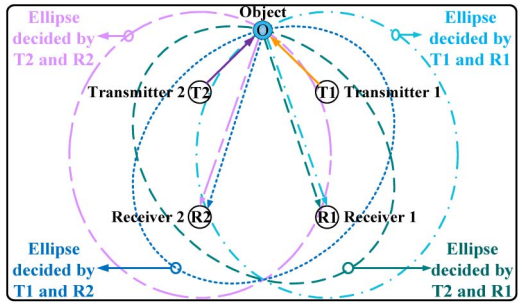

Fig. 2. Geometric model of two-dimensional localization with two transmitters and two receivers.

$$L_{\mathrm{OT}i}+L_{\mathrm{OR}j}=ct_{\mathrm{T}i\mathrm{R}j} \qquad i=1,2 \qquad j=1,2, \quad (2)$$

where c is the velocity of electromagnetic wave in the vacuum; L_{OT1} and L_{OT2} are the distances between the target and the transmitters 1 and 2, respectively; and L_{OR1} and L_{OR2} are the distances between the target and the receivers 1 and 2, respectively. $t_{\mathrm{T}i\mathrm{R}j}$, ($i=1,2$ and $j=1,2$) are the TOAs from the transmitter i to the receiver j. For a target with unknown position (x,y), denoting the coordinates of Transmitter 1, Transmitter 2, Receiver 1, and Receiver 2 as $(x_{\mathrm{T1}},y_{\mathrm{T1}})$, $(x_{\mathrm{T2}},y_{\mathrm{T2}})$, $(x_{\mathrm{R1}},y_{\mathrm{R1}})$, and $(x_{\mathrm{R2}},y_{\mathrm{R2}})$, respectively, a set of equations for ellipses can be achieved:

$$\sqrt{(x-x_{\mathrm{T}i})+(y-y_{\mathrm{T}i})}+\sqrt{(x-x_{\mathrm{R}j})+(y-y_{\mathrm{R}j})} = ct_{\mathrm{T}i\mathrm{R}j} \qquad i=1,2 \qquad j=1,2. \quad (3)$$

$(x_{\mathrm{T1}},y_{\mathrm{T1}})$, $(x_{\mathrm{T2}},y_{\mathrm{T2}})$, $(x_{\mathrm{R1}},y_{\mathrm{R1}})$, and $(x_{\mathrm{R2}},y_{\mathrm{R2}})$ are the known parameters since the positions of the transmitters and the receivers are known. The parameters $t_{\mathrm{T}i\mathrm{R}j}$, $i=1$, 2, $j=1$, 2, are the TOAs which can be obtained in the central station using a time delay estimation algorithm (e.g., adaptive time delay estimation method [14]). The system delays included in the TOAs obtained from the algorithm can be eliminated by delay calibration given that fiber lengths between the radar units and the central station is fixed. Therefore, no clock synchronization of the radar units is required.

By solving (3), the location of the target, i.e., (x,y), can be obtained. Since the equations are nonlinear, it is not easy to get the solution. The Taylor-series method [15] which is an iterative algorithm is applied in this work to obtain accurate position estimation. As can be seen in Fig. 2, two possible solutions may be achieved, but only one solution is effective if the UWB antennas used in the system are directional.

A proof-of-concept experiment is carried out for two-dimensional localization of a metal target using two transmitters and two receivers. A multi-channel laser source (Agilent N7714A) is used to generate four optical lightwaves with wavelengths of 1553.32, 1551.72, 1550.12,

and 1548.52 nm, which are assigned to Receiver 1, Receiver 2, Transmitter 1, and Transmitter 2, respectively. Two dense wavelength-division multiplexers (DWDMs) with 200 GHz channel spacing are used to multiplex and demultiplex the four channels, respectively. At each transmitter unit, a 10 GHz MZM, 1 km SMF, a 50:50 optical splitter, a PD with a bandwidth of 20 GHz, an EBPF with a bandwidth of 3.1–10.6 GHz, and a broadband EA (Agilent 83020A) with a bandwidth of 2–26.5 GHz are used. A 10 dB electrical coupler is used to introduce part of the chaotic signal to the emission UWB antenna. The UWB antenna has a working bandwidth of 3–18 GHz. At each receiver, a UWB antenna and a LNA with a gain of 40 dB are used. A four-channel 32 GHz digital storage oscilloscope (Agilent DSO-X 92504A) with a sampling rate of 40 GSa/s is used to record the waveforms at the output of the PDs in the central station.

Figures 3(a)–3(d) show the time sequence, power spectral density (PSD), amplitude histogram, and normalized auto-correlation trace of the chaotic signal generated from the chaotic OEO in each transmitter unit. As can be seen in Fig. 3(a), a time sequence of the generated chaotic signal with a duration time of 10 us is captured by the oscilloscope. The largest Lyapunov index of the sequence is calculated to be 1.2264 ns^{-1}, which confirms that the generated signal is a chaotic signal. The PSD of the signal is very flat in the range from 3.1 to 10.6 GHz, in accord with the passband of the EBPF used in the loop of the chaotic OEO, as shown in Fig. 3(b). The amplitude histogram of the chaotic signal and a Gaussian fitted curve are shown in Fig. 3(c). It can be seen that the amplitude histogram is of Gaussian-like statistics, showing that the generated chaotic signal has a good randomicity. From the normalized auto-correlation trace in Fig. 3(d), a narrow and sharp peak with no apparent side lobe can be seen. The full width at half maximum (FWHM) of the auto-correlation peak is 0.035 ns, as shown in the inset, indicating that the range resolution is equal to 1.05 cm. According to [3], the normalized cross-correlation level of the quasi-orthogonal waveforms should be at a level roughly equal to $-10\log(TB)$ dB, where T is the time length of the signal and B is the signal bandwidth. The chaotic signal captured by the oscilloscope has a 10 μs time length and a 7.5 GHz bandwidth; thus, the normalized cross-correlation level should be roughly equal to −48.8 dB. As can be seen in Fig. 3(e), the normalized cross-correlation level of the two emitted chaotic signals is nearly −45 dB, very close to the theoretical value of −48.8 dB, which demonstrates that the two chaotic signals generated from different chaotic OEOs are quasi-orthogonal.

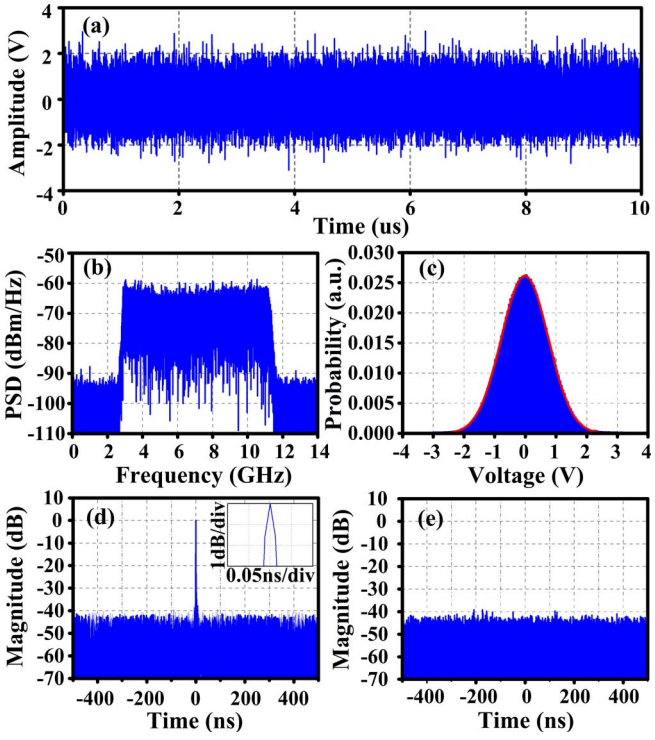

Fig. 3. (a) Time sequence, (b) power spectral density, (c) amplitude histogram, and (d) normalized auto-correlation trace of the chaotic signal generated by OEO. (e) Normalized cross-correlation trace of the two emitted chaotic signals.

To get the accurate time difference between the reference signal and the received signal, an adaptive time delay estimation algorithm is applied. With the algorithm, the position of the maximum weight coefficient in the weight vector corresponds to the time delay. Another issue is that the direct signals from the transmitters collected by the receiver would introduce strong interferences to the system, as shown in Fig. 4(a). To solve this problem, an adaptive filtering method [16] is used, which greatly suppresses the impact of the direct signal, as shown in Fig. 4(b). Since the chaotic signals are quasi-orthogonal, the emitted signal from each transmitter can be differentiated by using the corresponding reference signal.

Figure 5 shows the time delay estimation results with direct signal suppression. By searching the peaks, we can easily get that the time differences between Transmitter 1 and Receiver 1, Transmitter 1 and Receiver 2, Transmitter 2 and Receiver 1, and Transmitter 2 and Receiver 2 are 17.350 ns, 19.275 ns, 18.275 ns, and 20.075 ns, respectively. It should be noted that the estimated time delay includes system delay, which can be eliminated by delay calibration. By placing a target at a known position, the system delay between

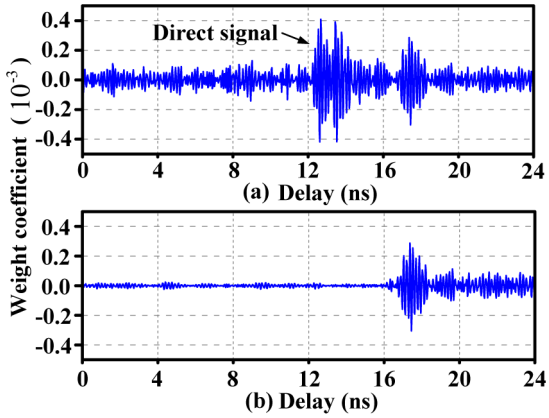

Fig. 4. Time delay estimation result (a) without and (b) with direct signal suppression.

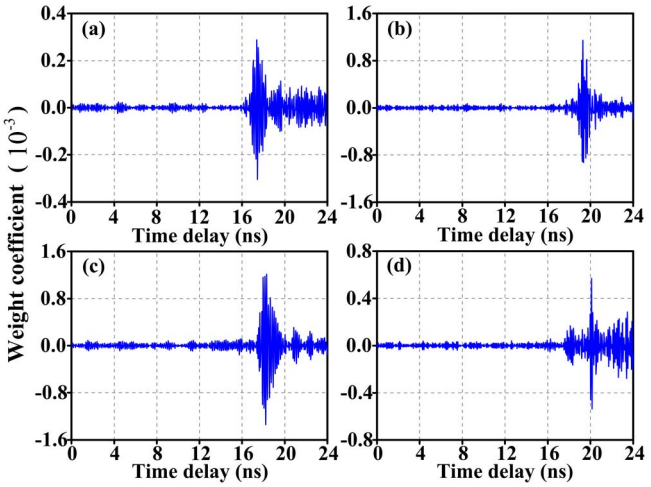

Fig. 5. Time delay estimation results with direct signal suppression for achieving TOAs between (a) Transmitter 1 and Receiver 1, (b) Transmitter 1 and Receiver 2, (c) Transmitter 2 and Receiver 1, (d) Transmitter 2 and Receiver 2.

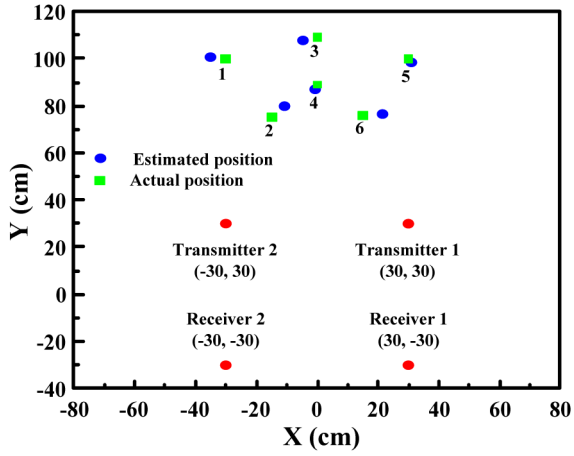

Fig. 6. Geometric locations of six samples of the estimated positions and their corresponding actual positions.

each transmitter and each receiver can be obtained by subtracting the true delay from the estimated one. Once the system delays are achieved, the actual TOAs will be obtained by subtracting the system delays from the estimated delays. With the TOAs and the given positions of the transmitters and the receivers, the location of the target is estimated to be (−0.62 cm, 86.98 cm). Being compared with the actual position of (0.00 cm, 89.00 cm), the localization error is 2.11 cm.

Table 1. Six Samples of the Actual Position and the Estimated Position of the Target

Sample	Actual Position	Estimated Position	Error (cm)
1	(−30.00, 100.00)	(−35.06, 100.64)	5.10
2	(−15.00, 75.00)	(−10.75, 79.80)	6.41
3	(0.00, 109.00)	(−4.61, 107.70)	4.79
4	(0.00, 89.00)	(−0.62, 86.98)	2.11
5	(30.00, 100.00)	(31.01, 98.40)	1.89
6	(15.00, 76.00)	(21.47, 76.46)	6.49

To further investigate the accuracy of the proposed localization system, measurements are performed with six different target locations. The six estimated positions and the corresponding actual positions are shown in Fig. 6, and the position values and the location errors are shown in Table 1. From Table 1, we can find that the maximum localization error of the system is 6.49 cm.

In conclusion, a distributed MIMO chaotic radar based on WDM technology is proposed and demonstrated. The multiple wideband quasi-orthogonal chaotic signals generated by using chaotic OEOs have a noise-like characteristic and good correlation property, which makes this kind of signal an excellent candidate for distributed MIMO radar application. Thanks to the low loss and wide bandwidth signal transmission in the WDM network, the proposed distributed MIMO chaotic radar has the ability to jointly process all the raw data from the receivers and the reference signals from the transmitters, which ease the requirement of precise clock synchronization and provide the possibility to move complex signal processing from each receiver to the central station. The experiment for two-dimensional localization of a metal target using two transmitters and two receivers shows that the system has the maximum position error of less than 6.5 cm.

This work was supported in part by the National Basic Research Program of China (2012CB315705), the National Natural Science Foundation of China (61201048, 61422108), the Natural Science Foundation of Jiangsu Province (BK2012381, BK2012031), and a Project Funded by the Priority Academic Program Development of Jiangsu Higher Education Institutions..

References

1. J. Li and P. Stoica, IEEE Signal Process. Mag. **24**(5), 106 (2007).
2. A. M. Haimovich, R. S. Blum, and L. Cimini, IEEE Signal Process. Mag. **25**(1), 116 (2008).
3. M. S. Willsey, K. M. Cuomo, and A. V. Oppenheim, IEEE Trans. Aerosp. Electron. Syst. **47**, 1974 (2011).
4. M. I. Jeong, J. N. Lee, and C. S. Lee, J. Electromagn. Waves Appl. **22**, 1725 (2008).
5. A. B. Wang, Y. C. Wang, and H. C. He, IEEE Photon. Technol. Lett. **20**, 1633 (2008).
6. S. S. Li, Q. Liu, and S. C. Chan, IEEE Photon. J. **4**, 1930 (2012).
7. M. J. Zhang, Y. N. Ji, Y. N. Zhang, Y. Wu, H. Xu, and W. P. Xu, IEEE Photon. J. **6**, 7902412 (2014).
8. Y. Ji, M. Zhang, Y. Wang, P. Wang, A. Wang, Y. Wu, X. Hang, and Y. Zhang, Int. J. Bifur. Chaos **24**, 1450032 (2014).
9. K. E. Callan, L. Illing, Z. Gao, D. J. Gauthier, and E. Schöll, Phys. Rev. Lett. **104**, 113901 (2010).
10. J. Y. Zheng, H. Wang, J. B. Fu, W. Li, S. L. Pan, L. X. Wang, J. G. Liu, and N. H. Zhu, Opt. Express **22**, 4896 (2014).
11. F. Y. Lin and J. M. Liu, IEEE J. Quantum Electron. **40**, 815 (2004).
12. J. B. Fu and S. L. Pan, Opt. Express **21**, 21218 (2013).
13. T. F. Yao, D. Zhu, S. F. Liu, F. Z. Zhang, and S. L. Pan, IEEE Photon. Technol. Lett. **26**, 1874 (2014).
14. F. A. Reed, P. L. Feintuch, and N. J. Bershad, IEEE Trans. Acoust., Speech, Signal Process. **29**, 561 (1981).
15. W. H. Foy, IEEE Trans. Aerosp. Electron. Syst. **AES-12**, 187 (1976).
16. P. Howland, D. Maksimiuk, and G. Reitsma, IEE Proc. Radar Sonar Navig. **152**, 107 (2005).